AURORAL KILOMETRIC RADIATION: TIME-AVERAGED SOURCE LOCATION

by

Dennis Gallagher

A thesis submitted in partial fulfillment
of the requirements for the degree of
Master of Science in Physics
in the Graduate College of
The University of Iowa

December, 1978

Thesis supervisor: Professor Donald A. Gurnett

Graduate College
The University of Iowa
Iowa City, Iowa 52242

CERTIFICATE OF APPROVAL

MASTER'S THESIS

This is to certify that the Master's thesis of

Dennis L. Gallagher

has been approved by the Examining Committee for the thesis requirement for the degree of Master of Science in Physics at the December, 1978, graduation.

Thesis committee: David A. Gurnett
Thesis supervisor

Glenn Joyce
Member

John Allen
Member

ACKNOWLEDGEMENTS

This thesis is the result of the encouragement, contributions, and support of the people who make up the Department of Physics and Astronomy at the University of Iowa. The student who comes to this department will find people who are willing to help the student learn and succeed. Their names will change, but it is their contributions to the professional growth of each student that make productive members of the scientific community.

My first experiences at the University of Iowa were influenced by James L. Green, whose enthusiasm led me to the VLF Space Physics group. Dr. Donald A. Gurnett accepted me into the group and entrusted me with the development of the physics which is the subject of this thesis. With the help of Thomas Hannemann and Robert Brechwald who ran computer programs that would not run, and advice and directions from James Green, William Kurth, Dr. Roger R. Anderson, Dr. Robert Shaw, Richard West, and Geary Voots, I have written this thesis. The clear professional format in which this thesis has been produced is the work of Sandy Van Engelenhoven and Kathy Goodner. The excellent drafting of the figures is the work of John Birkbeck, Joyce Chrisinger, and Jeana Wonderlich.

In all, I owe a tremendous debt to the people mentioned above and those others who have made my experience as a graduate student

enjoyable and rewarding. I am fortunate that my debt might be repaid by my enthusiastic participation in the growth of individuals and of science in this Department of Physics of the University of Iowa.

This work was supported in part by NASA contracts NAS5-11074, NAS5-11431 and NAS1-13129.

ABSTRACT

The location of the average generation region of auroral kilometric radiation (AKR) is found by studying average electric field strengths as a function of spacecraft position in narrow frequency bands centered at 178 kHz, 100 kHz, and 56.2 kHz. A combined five years of data from the University of Iowa plasma wave experiments on satellites Hawkeye-1 and IMP-6 provide the basis for determining the average electric field strengths. Hawkeye-1 was in a highly elliptical, polar orbit with an apogee near 21 earth radii over the northern polar region and IMP-6 was in a highly elliptical, near equatorial orbit with an apogee of 33 earth radii. Together these satellites provide extensive coverage from 3 R_e to 21 R_e in the northern hemisphere and inside of 3 R_e in the southern hemisphere. Intense sources of AKR are found in the northern and southern hemispheres. Their locations are near 65° invariant latitude in their respective hemispheres, between 22^h and 24^h magnetic local time, and near 2.5 earth radii. The total time-averaged power generation is found to be about 10^7 watts, assuming a spectral bandwidth of 200 kHz. Propagation effects limit the emission cone of AKR in a given hemisphere to roughly 4.1 steradians at 178 kHz, 2.2 steradians at 100 kHz, and 1.5 steradians at 56.2 kHz. Evidence that the polar

cusp region is illuminated at distances as close as four earth radii suggests the possibility that previously observed polar cusp sources are the result of scattering off of field-aligned scattering centers.

TABLE OF CONTENTS

LIST OF FIGURES

I. INTRODUCTION

This study of electric field intensities has been undertaken to resolve uncertainties in the location of intense sources of earth related kilometric radiation. From the earliest observations by Benediktov et al. [1965, 1968], evidence submitted by numerous investigators has pointed to widely varying locations for the origin of the very intense and sporadic kilometric radiation which has a sharply peaked spectrum between 100 and 300 kHz. The spectrum of this radiation is shown in Figure 1 and compared with free and trapped continuum radiation and the galactic spectrum [Gurnett, 1975]. Benediktov et al. [1965, 1968] correlated radio emissions between 0.725 and 2.3 MHz with geomagnetic activity and concluded that the source is near the earth. Dunckel et al. [1970] reported that this intense radiation is observed primarily in the local evening and is strongly correlated with the auroral electrojet (AE) index. A source location in the tail region of the magnetosphere for sporadic noise at 250 kHz was observed by Stone [1973]. Gurnett [1974] presented a frequency of occurrence study of kilometric radiation showing a conical radiation pattern centered at the earth, at high latitudes in the local evening, and referred to this intense radiation as terrestrial kilometric radiation (TKR). Gurnett showed that the qualitative ray paths drawn in Figure 2 could explain the observed conical

radiation pattern, if the source location of the radiation was on an auroral field line at $\leq 3\ R_e$ (earth radii). The two-component source model proposed by Kaiser and Stone [1975] described a less intense, quasi-continuous dayside source in addition to the intense, sporadic nightside source described by Gurnett. Using the direction finding technique of analyzing spin modulated electric field intensities from satellites Hawkeye-1 and IMP-8, Kurth et al. [1975] reported the average source location of auroral kilometric radiation (AKR) between 1 and 2 R_e and at about 20^h magnetic local time. The satellite's antenna orientation at a null in strongly spin-modulated electric field intensities gives the direction to the source region. Such measurements together with others were used to triangulate on the centroid of the emitting region (Figure 3). In another experiment, lunar occultations of intense kilometric radiation observed with RAE-2 were used by Kaiser and Alexander [1976] to locate apparent source origins (Figure 4). The most intense source observed was the AKR source described by Kurth et al. [1975]. Also observed were emissions in the region of the polar cusp and magnetosheath on the dayside and associated with regions of the magnetotail in the night hemisphere.

Such diverse observations of the source locations of this intense kilometric radiation have produced the very difficult task of finding a single mechanism for the generation of the radiation, which will operate under widely varying plasma conditions. Toward resolving the dilemma, Alexander et al. [1978] have recently given

strong evidence that kilometric radiation generated near the earth at auroral latitudes may be scattered at large distances in the magnetosheath and solar wind, thereby appearing to come from distant sources. Following this explanation of the observation of distant kilometric radiation sources, two types of TKR observations remain to be examined. The strongest component is AKR, which is known to originate within 5 R_e, at auroral latitudes, and in the local evening. Other less intense components discussed by Alexander et al. [1978] are observed between 5 and 15 R_e and appear to come from sources aligned along a specific family of geomagnetic field lines. An example is the polar cusp sources observed by Kaiser and Alexander [1976]. In summary, these studies have found source locations by lunar occultation techniques and by examining spin-modulated electric field intensities. The methods determine the instantaneous positions of apparent sources of intense kilometric radiation. Such an apparent source may represent a generation region of the radiation or scattering off of a localized inhomogeneity in plasma density.

The present study will determine which regions in the magnetosphere are strong sources of power at kilometric wavelengths. Time-averaged spectral power flux will first be integrated over earth-centered spherical shells. For shells of varying radius the integrals will give the spectral power and geocentric radial distance of regions of power generation. The latitudinal and local time dependences of the averaged spectral power flux will be examined along with a consequence of the $1/R^2$ radial dependence of spectral power flux

observed by Gurnett [1974] for TKR. As postulated by Alexander et al. [1978], previously observed polar cusp sources may result from field-aligned scattering centers. This study is not sensitive to the effects of the scattering or reflection of electromagnetic radiation. Only regions of power generation at kilometric wavelengths will be observed. The dimensions of observed regions of power generation will also be a measure of the variation in the locations of instantaneous intense sources of kilometric radiation. To the extent that this study better defines those regions which contribute to the energy produced at kilometric wavelengths, the generation mechanism for intense kilometric radiation may be sought using a more limited range of plasma parameters than has been possible in the past.

II. INSTRUMENTATION

The Hawkeye-1 and IMP-6 satellites have similar plasma wave experiments which together have provided about five years of electric field measurements. The combined orbital coverage of the satellites is shown in Figure 5. Locations where measurements are made on the nightside of the earth have been rotated in magnetic local time to form the right side of the figure; all points on the dayside have been rotated to form the left side of the figure. As shown, northern hemisphere coverage is almost complete out to about 21 R_e. There is no coverage, however, at small radial distances and at high latitudes above the northern pole. Southern hemisphere coverage is limited to latitudes greater than about -40° magnetic latitude, except for Hawkeye-1 coverage within 2 R_e.

The Hawkeye-1 satellite was launched into a highly elliptic orbit in June, 1974 and re-entered the atmosphere in April, 1978. Initial perigee and apogee in earth-centered radial distances were 6,847 and 130,856 km respectively. The orbit was inclined 89.81° with respect to the equatorial plane. The spacecraft was spin stabilized with a spin period of about 11 seconds, oriented with its spin axis approximately in the plane of the initial orbit.

The plasma wave experiment on Hawkeye-1 consisted of a very narrow band "step-frequency receiver" connected to an electric dipole

antenna. The electric dipole antenna was extended to a tip-to-tip length of 42.45 meters, perpendicular to the axis of rotation. The 16 narrow band channels ranged in center frequency from 1.78 Hz to 178 kHz. The system equivalent noise bandwidth was approximately 5% of the center frequency for the upper eight channels of the receiver. The output of each band pass filter was fed to a log compressor which compressed an input dynamic range of 100 db into an output signal of 0 to 5 volts. This output voltage is approximately proportional to the logarithm of the electric field intensity. A more complete description of the plasma wave experiment was given by Kurth et al. [1975].

The IMP-6 spacecraft was also launched into a highly elliptical orbit and flew from March, 1971 until burn-up in the atmosphere in October, 1974. Initial perigee and apogee in earth-centered distances were 6,610 and 212,630 km respectively. Orbital inclination was 28.7° with respect to the equatorial plane. The spacecraft was spin stabilized with a period of about 11 seconds, with its spin axis oriented perpendicular to the ecliptic plane.

The plasma wave experiment on IMP-6 was described by Gurnett and Shaw [1973] and is very similar to Hawkeye-1. The tip-to-tip antenna length was 92.5 meters. The very low frequency receiver consisted of 16 narrow frequency band filters covering the frequency range from 35.5 Hz to 178 kHz. For the upper three channels, the system equivalent noise bandwidth was approximately 10% of each center frequency. Each receiver produced an output voltage of

0 to 5 volts, which is nearly proportional to the logarithm of the input signal amplitude over a dynamic range in excess of 100 db.

The success of integrating spectral power flux over spherical shells to find regions of power generation, depends strongly upon the completeness of the flux observations over each spherical surface. Such observations cannot satisfactorily be provided by the data from only one satellite. The orbital coverage of satellites Hawkeye-1 and IMP-6 are only partially overlapping. When taken together, the data from these satellites provide an extensive survey of electric field strengths in the vicinity of the earth. Although not shown in Figure 5, the combined orbital coverage extends uniformly throughout all magnetic local times.

III. DATA ANALYSIS

Integrating average power flux over earth-centered spherical shells will give an estimate of the geocentric radial distances of the sources of the most intense kilometric radiation and the value of the total average power generation. Using simultaneous observations of electric and magnetic fields by IMP-6, Gurnett [1974] showed that electric to magnetic field ratios of intense kilometric radiation correspond to that for electromagnetic waves in free space. On this basis, an inverse dependence of power flux on the square of radial distance should be observed in the data obtained from satellites Hawkeye-1 and IMP-6. However, the $1/R^2$ dependence of power flux on distance should be seen only as a function of the distance from the origin of the radiation. This origin may be inferred by selecting a source region which yields the power flux dependence of $1/R^2$ that is expected for free space propagating electromagnetic radiation.

Measurements of electric field strength, by each satellite, are logarithmically compressed and available in the form of a voltage between 0 and 5 volts (V_{out}). Using prelaunch calibration tables, these measurements are converted to the actual voltages applied to the satellite antennas (V_{in}). With effective antenna lengths and filter bandwidths, the electric field strength and spectral power flux can be calculated for each measurement using:

$$E = \frac{V_{in}}{L_{eff}}$$

$$P = \sqrt{\frac{\epsilon_o}{\mu_o}} \frac{E^2}{\Delta f_{eff}} K^2$$

K = correction factor for antenna capacitance voltage losses

V_{in} = antenna potential

Δf_{eff} = effective bandwidth

L_{eff} = effective antenna length

Because Gurnett [1974] found that voltage attenuation due to antenna capacitance had a small effect on the measurement of electric field strengths, K is assumed to be approximately equal to one. Based on spin rates, the electric field data from Hawkeye-1 and IMP-6 are averaged over $3^m\ 4^s$ and $5^m\ 28^s$ intervals respectively, and as a consequence, spin modulation is removed from the data. In a study by Green et al. [1976], the calibrations on these two satellite instruments were compared through simultaneous observations of type-III radio bursts. On the assumption that the satellites were equidistant from the source regions of type-III radio bursts, the observations of electric field strengths were found to be in close agreement; therefore, no normalization is required in averaging measurements of spectral power flux by the two satellites. All data are averaged into 72 five-degree increments of magnetic local time (MLT), 36 five-degree increments of magnetic latitude (λ_m), and 15 equal logarithmic increments in geocentric radial distance. This produces a picture of time-averaged spectral power fluxes as a function

of position in the vicinity of the earth. The resolution of the picture is limited only by the amount of data available from Hawkeye-1 and IMP-6. For the chosen resolution, there are 10 to 50 measurements of spectral power flux averaged into each volume element where satellite coverage exists. The objective is for the average of spectral power flux measurements within each volume element to be representative of the average kilometric radiation intensities at each corresponding location. Bursts of TKR last from tens of minutes to several hours. As a result, some observations within a given volume element will be made when TKR cannot be observed. By requiring many measurements within a volume element, numerous observations of TKR will occur and the average of all measurements will approach the value of the average intensity of TKR at the corresponding locations.

As described, electric field data from satellites Hawkeye-1 and IMP-6 are averaged over $3^m\ 4^s$ and $5^m\ 28^s$ intervals respectively. These averages produce over 600,000 measurements of spectral power flux. Because sources of radiation at kilometric wavelengths such as continuum radiation and type-III radio bursts have been observed by Gurnett [1974] to be a minor source of energy when compared to TKR, no lower threshold on measurements of spectral power flux will be used to exclude these other forms of kilometric radiation from the present study. An upper threshold can be established at respective receiver channel saturations and results in the omission of only four measurements.

Also important is how well measurements of spectral power flux represent the spectral components of the magnitude of the poynting flux. How well an average across the spin-modulated data corresponds to the magnitude of the poynting flux depends ideally on the polarization of the radiation and the orientation of the satellite's axis of rotation. For radiation linearly polarized in the satellite's plane of rotation, the observed electric field strength will vary with a peak-to-peak amplitude equal to that of the electric field component of the radiation. An average of electric field measurements will give a result which is about 0.7 times the actual electric field strength. Electric field measurements will be equal to zero for radiation linearly polarized in the direction of the satellite's axis of rotation. The average of measurements of circularly polarized radiation will yield a result which varies approximately from a factor of 1 to 0.7 times the magnitude of the electric field component of the radiation. The larger result occurs when the poynting flux direction is along the satellite's axis of rotation. AKR is an R-X mode propagating radiation as predicted by Green et al. [1976] and observed by Gurnett and Green [1978] and by Kaiser et al. [1978]. Each electric field average will be in error by no more than a factor of about 1.4 and, therefore, spectral power flux measurements will be in error by no more than a factor of about two. However, the errors are systematic in nature and should not influence the process of locating the AKR source, which depends upon relative spectral flux magnitudes.

The present study could also be influenced by seasonal and long-term time variations in kilometric radiation intensities. Seasonal changes are sought by studying separate summer and winter averages of spectral power flux as a function of position. When plots along earth-centered radial vectors of spectral power flux versus distance are made separately for the summer and winter, no statistical differences are found. A possible source of long-term variations is the 11-year solar sunspot cycle. Data are taken from satellites IMP-6 and Hawkeye-1, which provide seven years of almost non-overlapping temporal coverage. A solar minimum occurred midway through those seven years, therefore, measurements from these two satellites were made during similar phases of the solar cycle. The effect is expected to mask solar cycle related variations in kilometric radiation intensities. Consequently, the data examined in this study constitutes, as well as possible, an unbiased representation of spectral power flux intensities in the vicinity of the earth.

Assume initially that the picture proposed by Gurnett [1974], which is shown in Figure 2, is generally accurate in describing the locations of the most intense sources of kilometric radiation. The sources of intense kilometric radiation are shown in the figure to be very close to the earth and at high latitudes on auroral field lines. If these northern and southern sources of auroral kilometric radiation (AKR), as termed by Kurth et al. [1975], are well confined then an integration of the poynting flux over spherical shells

which completely enclose the source regions should yield a constant power result as shown in Figure 6. If both sources could always be seen, this constant result would be equal to the total spectral power generated at the frequency for which the data were chosen. As the radius of these concentric, spherical, earth-centered shells become small, a radius will be reached where they no longer completely enclose the generation regions. As this occurs, the integrated power will fall off at a rate which reflects how well, on the average, the source is confined radially. The radii of shells during which this drop off occurs define the location of the source regions in earth-centered radial distance. Poynting flux, however, is not available from both satellites. Instead, measurements of average spectral power flux are used to perform the integrations:

$$\int_{\text{sphere}} \vec{S} \cdot d\vec{A} \approx \int P \, dA = \sqrt{\frac{\epsilon_o}{\mu_o}} \frac{1}{\Delta f} \int \overline{E^2} \, dA$$

$$\sqrt{\frac{\epsilon_o}{\mu_o}} \approx \frac{1}{377}$$

$\vec{S}$ = Spectral poynting vector

P = Spectral power flux

The effect of introducing this approximation will be discussed later.

As described above, power flux is averaged within volume elements of 5 degrees MLT, 5 degrees λ_m, and 15 radial distance increments. To perform the integration, all volume elements must

contain a measurement of spectral power flux. Orbital coverage, however, was not 100% complete, as shown in Figure 5. To compensate, those volume elements for which there is no satellite data are filled with the average spectral power flux calculated from all those volume elements which contain satellite data. As noted, incomplete orbital coverage occurred primarily in the southern hemisphere. The procedure for artificially filling volume elements with data, therefore, depends mostly upon the symmetry between the northern and southern hemispheres. This filling procedure is used because symmetry is found between the northern and southern hemispheres when existing spectral power flux measurements are examined. Finally, volume elements within each radial distance increment are treated as spherical shells with radii which are the average for all measurements within each radial group.

The integration was then performed for 178, 100, and 56.2 kHz and the result is shown in Figure 7. Each of the radial distances plotted represents an average of the radial distances of the measurements in each corresponding radial distance group. The lower panel in Figure 7 shows the extent of satellite orbital coverage as a percentage of 4π steradians. The error bars in the figure represent the standard deviation [$\sigma(P)$] of the integration for each of 15 spherical shells at each frequency. This error was calculated from the standard deviation of the measurements of spectral power flux [$\sigma(p)$] and of radial distance [$\sigma(r)$] on each spherical surface of integration, with the expression:

$$\sigma(P) = \left\{\left(\frac{\partial P}{\partial \overline{p}}\right)^2 [\sigma(\overline{p})]^2 + \left(\frac{\partial P}{\partial \overline{r}}\right)^2 [\sigma(\overline{r})]^2\right\}^{1/2}$$

$$P = \int_{\text{sphere}} p\,dA = \sqrt{\frac{\varepsilon_o}{\mu_o}}\,\frac{1}{\Delta f}\int_{\text{sphere}} E^2\,dA$$

$$\overline{p} = \sum_{i=1}^{N} p_i/N$$

$$\overline{r} = \sum_{i=1}^{N} r_i/N$$

p_i = average spectral power flux in solid angle element dA_i

r_i = average radius of solid angle element dA_i

N = number of solid angle elements where satellite coverage exists

where $\sigma(\overline{p})$ and $\sigma(\overline{r})$ were calculated from the general expression:

$$\sigma(\overline{A}) = \left\{\sum_{i=1}^{N} (A_i - \overline{A})^2/N(N-1)\right\}^{1/2}.$$

An interpretation of Figure 7 will be made later in the discussion section of this paper.

Another approach is to examine the data for $1/R^2$ propagation. Except for the plasmasphere propagation effects discussed by Green et al. [1974], auroral kilometric radiation propagates away from the earth in free space. The radiation should, therefore, propagate away from the source region with a $1/R^2$ radial dependence. A plot of average power versus earth-centered radial distances along

a radial vector that passes through the source region in a given hemisphere can easily be examined for the $1/R^2$ radial dependence. Prior to selecting a radial vector direction for making this plot, the southern and northern hemispheres are examined for symmetry. As discussed, they are found to be roughly equivalent in structure, therefore, the southern hemisphere data can be reflected about the equatorial plane and averaged together with northern hemisphere data to produce a single hemisphere of data with increased orbital coverage.

Because these data are organized in earth-centered coordinates, average spectral power flux can not easily be examined for $1/R^2$ radial dependence until a solid angle is chosen which passes as near as possible to the source region. For the selection of such a solid angle, the dependence of spectral power flux on distance may be examined in a single dimension along the corresponding radial vector. The solid angle direction is chosen by examining the MLT and λ_m dependence of the intensity of the radiation. Figure 8 shows intensity modulated, polar plots of power flux for four radial distance groups. The logarithm of spectral power flux is used to determine the darkness of the plot. The more intense fluxes correspond to the darker regions in each plot. The plots appear to show a cone of emission originating from pre-midnight magnetic local times and at intermediate magnetic latitudes. The magnetic latitudes of the solid angle which must be determined, are selected to range from 30° and 55°. This selection of magnetic

latitudes is large enough to include the location of the source region, and small enough to avoid the areas of poor orbital coverage at high latitudes.

The MLT dependence is examined in two ways. For six radial distance groups, the average power is integrated across the magnetic latitudes chosen above for 24 magnetic local times. The resulting plots for 178, 100, and 56.2 kHz are shown in Figures 9, 10, and 11, respectively. In each plot, the logarithm of spectral power is plotted against MLT for six radial distance groups. The cone-like emission of the radiation appears to originate between 22^h and 24^h MLT for the three frequencies. Also seen on these plots at small radial distances are features which do not appear to follow the cone-like emission pattern of the intense kilometric radiation under study. These features are believed to represent other forms of energy at kilometric wavelengths such as auroral hiss and electrostatic plasma oscillations. They are not excluded from these observations because they do not effect this study of intense kilometric radiation. Another approach to the selection of a MLT direction is to directly plot average power versus earth-centered radial distances in various MLT directions. The MLT which best corresponds to that of the source region will show the most intense and most sharply peaked plot because measurements along a radial vector in that MLT will pass closer to the source region than in any other MLT. Plots made in four MLT groups for spectral power fluxes averaged between 30° and 55° λ_m are shown in Figure 12. On the

basis of the above discussion, the plot between 22^h and 24^h MLT clearly represents the MLT direction of the source region. The peaks for plots in other magnetic local times are less intense and flattened because those points on a flattened peak represent locations which are separated and approximately equidistant from the source region. The solid angle has now been chosen to range from 22^h to 24^h MLT and from 30° to 55° λ_m. This selection best represents the direction of the source region from the center of the earth and avoids the influence of poor orbital coverage at high magnetic latitudes.

The plot in Figure 12 between 22^h and 24^h MLT can now be examined for $1/R^2$ radial dependence. A straight line fit to the trailing edge of the plotted curve for 178 kHz on this log-log graph has a slope of -3.47. Radial distances plotted on the graph are geocentric rather than distances from the source region, thereby increasing the slope of the straight line fit. The distance of the actual source region from the center of the earth can indirectly be found by re-plotting spectral power flux where the radial distances used are with respect to various possible source locations. An assumed source location which produces the expected slope of -2.0 when spectral power flux is plotted as a function of the distance from this location would then correspond to the actual distance of the source from the center of the earth. An example of the effect of choosing source locations at 2, 3, and 4 R_e for the frequencies

examined is shown in Figure 13. The dashed line in each plot represents a $1/R^2$ slope. As possible source locations are chosen at consecutively larger distances from the center of the earth, the slope reduces on these log-log plots. A uniform plot of slope as a function of source location is shown in Figure 14. The horizontal dashed line representing a $1/R^2$ slope shows an inferred actual source location which ranges from 2 to 3 R_e.

IV. DISCUSSION

The calculation of spectral power emitted at kilometric wavelengths by means of integrating over earth-centered, spherical shells was performed so that the radial distance of the most intense sources of kilometric radiation could be found. The result of the integration in Figure 7 agrees remarkably well with the ideal result shown in Figure 6. In many respects, however, the result shown in Figure 7 is not the product of ideal conditions. First, $\vec{S} \cdot d\vec{A}$ was approximated with the measured spectral power flux PdA or $\sqrt{\frac{\varepsilon_o}{\mu_o}} \frac{E^2}{\Delta f} dA$. As a measurement of the spectral poynting flux magnitude $|\vec{S}|$, the spectral power flux has been shown to be no more than a factor of about two too small. As a result of the approximation the magnitude of the component of the poynting flux normal to the surface of integration is not known. This means that the total observed spectral power flux magnitude will be used in the integration at each surface element. When the surface of integration has a large radius and completely encloses the source regions, the approximation should produce little effect and the result of the integration should be constant. As the surfaces of integration no longer completely enclose the source regions, the integral will become roughly proportional to the area of the surface of integration. Of importance is that the value of

the integral will deviate from a constant value when the radius of the surface of integration becomes less than the distance of the source positions from the center of the earth. This happens in Figure 7 at approximately 4 R_e. An additional reduction in the value of the integral occurs due to the proximity of the propagation cutoff surface, described by Gurnett [1974], which is located at about 2 R_e for high latitudes. For the radiation to be free space propagating, the source of intense kilometric radiation must be outside of the propagation cutoff surface, while the integration of spectral poynting flux places the source region inside of 4 R_e. The primary result of the integrations, therefore, locates well confined, intense sources of kilometric radiation, with apparent symmetry between the northern and southern hemispheres, at a distance of 2 to 4 R_e from the center of the earth. These are the northern and southern hemisphere AKR sources. No source of power at kilometric wavelengths is seen between 5 and 15 R_e.

A measurement of the total power emitted as AKR can also be determined. The significance of various features of the curves in Figure 7 must be examined before the power emitted as AKR can be obtained. Where orbital coverage becomes poor, the error in the integration becomes very large. The error for radial distances less than 3 R_e does not significantly effect the determination of source position because the reduction in the value of the integral remains clearly indicated near 4 R_e. Due to the large errors at distances

beyond 21 R_e, the sharp rise in the value of the integral cannot be reliably interpreted. It is possible that the sharp rise in the integrated power at distances beyond 21 R_e is caused by both reduced orbital coverage and the simultaneous observation of both northern and southern hemispherical sources on the nightside of the earth. At this distance, the solid angle where both sources are observable becomes a significant fraction of all solid angles where orbital coverage exists. An observation of spectral power flux is twice as large as that for the observation of only one source. Because the average of spectral power flux from those volume elements where coverage exists is used to fill those volume elements where orbital coverage does not exist, the value of the integration of spectral power flux across all solid angles may become larger than for the case when both sources could not be simultaneously observed. The slight downward slope of the curves in Figure 7 between 4 and 21 R_e appears to result from the procedure used to compensate for incomplete orbital coverage. As the radius of the spherical surface of integration increases, the satellite coverage in the southern hemisphere changes from positions near the source at intermediate latitudes to positions far from the source at more equatorial latitudes. When data from these southern hemisphere latitudes are averaged into existing northern hemisphere data, the resulting average first overestimates and then underestimates the average of the spectral power flux intensities where there is no orbital coverage. The value of the integration is first above and then below the unbiased value.

That portion of the curves in Figure 7 between 4 and 20 R_e has been averaged to estimate the power produced by one of the sources of AKR. The time-averaged spectral powers produced as AKR are approximately 37 Watts/Hz at 178 kHz, 16 Watts/Hz at 100 kHz, and 2 Watts/Hz at 56.2 kHz. If a spectrum bandwidth of 200 kHz is assumed for AKR emission, the total time-averaged power generation by one source is nearly 10^7 watts. Although these are order of magnitude estimates, they agree with an estimate of average power generation by Kaiser and Alexander [1977], and are compatible with an estimate of the peak power generation of 10^9 watts made by Gurnett [1974].

Auroral kilometric radiation is a free escaping radiation with a poynting flux magnitude which has been observed [Gurnett, 1974] to decrease as the inverse of the distance away from the source squared. The other approach to determining the AKR source location is to examine the data for $1/R^2$ radial dependence. Because available data are not based on an AKR source-centered coordinate system, the most convenient way to examine spectral power flux for $1/R^2$ dependence is to study only those data which occur within an earth-centered solid angle that passes through the source region.

As described before, the latitudes for the solid angle are chosen between 30° and 55° λ_m or between 57° and 69° invariant latitude. These latitudes are compatible with the 65° to 70° invariant latitude, which have been found for the AKR source location by Kurth et al. [1975]. Two approaches are

used to locate the source of AKR in MLT. In addition to finding magnetic local times for the source position centered between 22^h and 24^h, Figures 9, 10, and 11 show an increase in the size of the cone of illumination for AKR with increasing frequency. This confirms the dependence of the size of the AKR cone of emission on frequency that was observed by Green et al. [1976]. Once the solid angle is chosen, the results of searching for the effective source location are shown in Figures 13 and 14. Figure 14 shows that radiation from sources located at 2 to 3 R_e display the $1/R^2$ propagation. The error bars in Figure 14 represent the standard deviation of straight line fits to log-log plots such as those in Figure 13. This error results from the statistical error in the plotted points and the incorporation of electric fields in the data which are not related to AKR. Although the errors are enough that no significance can be drawn from the ordering of the curves in Figure 14, the AKR source location is found to be very near the earth, between 2 and 3 R_e, in agreement with the result derived from integrations of spectral power flux.

In addition to source strength and position, a striking feature of AKR is the broad angular emission pattern. The intensity modulated plots, like those in Figure 8, have been used to derive a sketch of the emission cone at 178 kHz. Figure 15 shows the cone of emission in the 11^h-23^h MLT plane overlayed on the Hawkeye magnetic field model of Chen and Van Allen [1978]. The plasmasphere shown in the sketch extends to L = 4 and is intended to correspond to an average KP index

of 3+. The borders of the emission pattern are defined by a drop of two or more orders of magnitude in the observed spectral power flux for each spherical shell into which the data has been averaged. The emission pattern is almost 180° wide in the dawn-dusk plane, crosses the equatorial plane near 12 R_e on the nightside of the earth, and is as low as 45° λ_m at 10 R_e on the dayside. Ray tracing in a model plasmasphere of L = 4 for a source at 2.3 R_e and 178 kHz was performed by Green [private communication, 1978] and confirms the sketch in Figure 15. By examining spectral power flux also at 100 and 56.2 kHz, the solid angles of the illumination patterns are found to be about 4.1 steradians at 178 kHz, 2.2 steradians at 100 kHz, and 1.5 steradians at 56.2 kHz. These emission cone solid angles are comparable to those found by Green et al. [1977], who developed frequency of occurrence pictures in MLT and λ_m for the observations of AKR. Using a drop in the frequency of occurrence to 50% to define emission cone boundaries, Green found emission cone solid angles of 3.5 sr at 178 kHz, 1.8 sr at 100 kHz, and 1.1 sr at 56.2 kHz.

Only the northern and southern hemisphere AKR sources are clearly observed using these methods of analysis. They are well confined near 65° invarient latitude in their respective hemispheres, from 22^h to 24^h MLT, and between 2 and 4 R_e. On average, instantaneous sources of AKR must also be confined within this region, because it is the variation in the location of instanteous sources of AKR which gives the appearance of an extended region of power generation.

No sources of power are evident in Figure 7 between 5 and 15 R_e. As discussed, the downward slope in the figure results from using the average of observed spectral power flux on a given shell as a substitute for actual spectral power flux values where there are no observations. The largest statistical error in the integration between 5 and 15 R_e for 178 kHz is approximately $\pm$ 20%. To be observed in this region of Figure 7, a source of electromagnetic radiation at 178 kHz would need to generate power equal to or greater than 20% of the power generated as AKR. Observations of dayside sources at distances greater than 5 R_e by Kaiser and Stone [1975] show that the flux from these sources is much less than that from AKR. These sources are too weak to be observed by this study. A more detailed study of the characteristics of the integration of spectral power flux is needed before the nature of TKR sources between 5 and 15 R_e can be determined. However, the observed illumination of the polar cusp at distances as small as 4 R_e allows observations of polar cusp sources, such as those by Alexander and Kaiser [1976], to be explained by field-aligned scattering centers.

CONCLUSIONS

Intense sources of power radiating at kilometric wavelengths are found near 65° invariant latitude in the northern and southern hemispheres, from 22^h to 24^h MLT, and between 2 and 4 R_e. These dominant sources of power produce the electromagnetic radiation that has been described by Kurth et al. [1976] as auroral kilometric radiation (AKR). Each northern and southern hemisphere AKR source is well confined and emits radiation into solid angles of about 4.1 sr at 178 kHz, 2.2 sr at 100 kHz, and 1.5 sr at 56.2 kHz. A lower limit for the spectral power generated by each source is found to be 37 Watts/Hz at 178 kHz, 16 Watts/Hz at 100 kHz, and 2 Watts/Hz at 56.2 kHz. For a bandwidth of 200 kHz, the total time-averaged power emitted by one source of AKR is found to be about 10^7 Watts.

LIST OF REFERENCES

Alexander, J. K., and M. L. Kaiser, Terrestrial kilometric radiation, 1. Spacial structure studies, J. Geophys. Res., 81, 5948, 1976.

Benediktov, E. A., G. G. Getmantsev, N. A. Mityakov, V. O. Papoport, and A. F. Tarasov, Relation between geomagnetic activity and the sporadic radio emission recorded by the Elektron satellites, Cosmic Research, English transl., 6, 791, 1968.

Benediktov, E. A., G. G. Getmantsev, Yu. Al. Sazonov, and A. F. Tarasov, Preliminary results of measurement of the intensity of distributed extraterrestrial radio-frequency emission at 725 and 1525-kHz frequencies by the satellite Elektron-2, Cosmic Research, English transl., 3, 492, 1965.

Chen, Tsan-Fu and J. A. Van Allen, The Earth's magnetic field at large radial distances as observed by Hawkeye-1, J. Geophys. Res., (submitted for publication, 1978).

Dunckel, N., B. Ficklin, L. Rorden, and R. A. Helliwell, Low-frequency noise observed in the distant magnetosphere with OGO 1, J. Geophys. Res., 75, 1854, 1970.

Green, J. L., D. A. Gurnett, and S. D. Shawhan, The angular distribution of auroral kilometric radiation, J. Geophys. Res., 82, 1825, 1977.

Gurnett, D. A., The Earth as a radio source: Terrestrial kilometric radiation, J. Geophys. Res., 79, 4227, 1974.

Gurnett, D. A., The Earth as a radio source: The nonthermal continuum, J. Geophys. Res., 80, 2751, 1975.

Gurnett, D. A., and J. L. Green, On the polarization and origin of auroral kilometric radiation, J. Geophy. Res., 83, 689, 1978.

Gurnett, D. A., and R. R. Shaw, Electromagnetic radiation trapped in the magnetosphere above the plasma frequency, J. Geophys. Res., 78, 8136, 1973.

Kaiser, M. L., and J. K. Alexander, Terrestrial kilometric radiation, 3. Average spatial properties, J. Geophys. Res., 82, 3273, 1977.

Kaiser, M. L., R. G. Stone, Earth as an intense planetary radio source: Similarities to Jupiter and Saturn, Science, 189, 285, 1975.

Kaiser, M. L., J. K. Alexander, A. C. Riddle, J. B. Pearce, and J. W. Warwick, Direct measure of the polarization of terrestrial kilometric radiation from Voyagers 1 and 2, J. Geophys. Res., (submitted for publication, 1978).

Kurth, W. S., M. M. Baumback, and D. A. Gurnett, Direction-finding measurements of auroral kilometric radiation, J. Geophys. Res., 80, 2764, 1975.

Stone, R. G., Radio physics of the outer solar system, Space Sci. Rev., 14, 534, 1973.

APPENDIX 1: FIGURES

Figure 1 The frequency spectrum of auroral kilometric radiation is shown against the galactic spectrum and the spectrums for trapped and free-escaping continuum radiation [Gurnett, 1975].

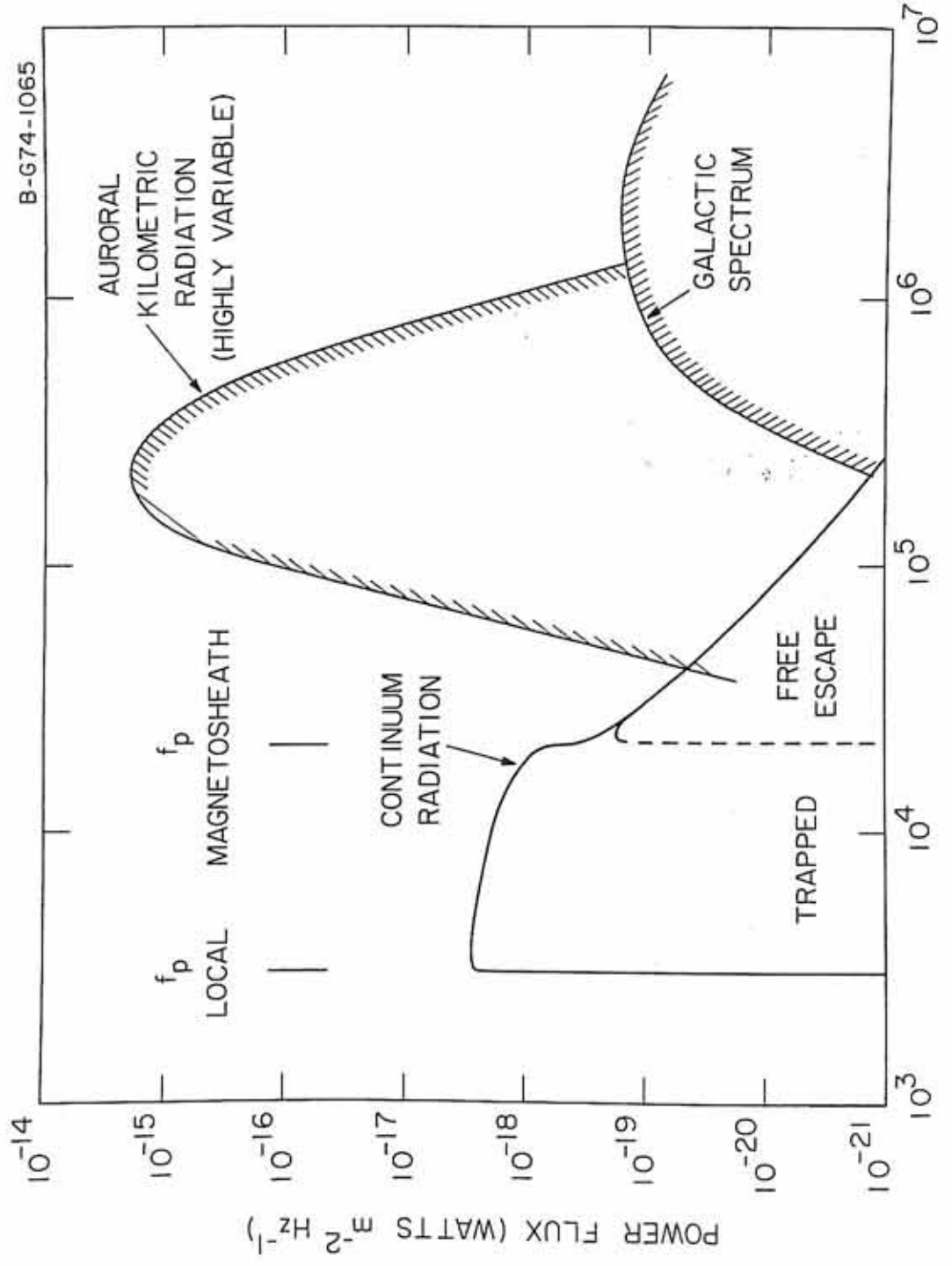
B-G74-1065
AURORAL KILOMETRIC RADIATION (HIGHLY VARIABLE)
GALACTIC SPECTRUM
f_p MAGNETOSHEATH
f_p LOCAL
CONTINUUM RADIATION
FREE ESCAPE
TRAPPED
POWER FLUX (WATTS m^{-2} Hz^{-1})
FREQUENCY (Hz)
10^{-14}
10^{-15}
10^{-16}
10^{-17}
10^{-18}
10^{-19}
10^{-20}
10^{-21}
10^{3}
10^{4}
10^{5}
10^{6}
10^{7}

Figure 1

Figure 2 This is a qualitative model by Gurnett [1974] of auroral kilometric radiation and of ray paths of electromagnetic radiation emitted at low altitudes and fixed frequency along an auroral field line.

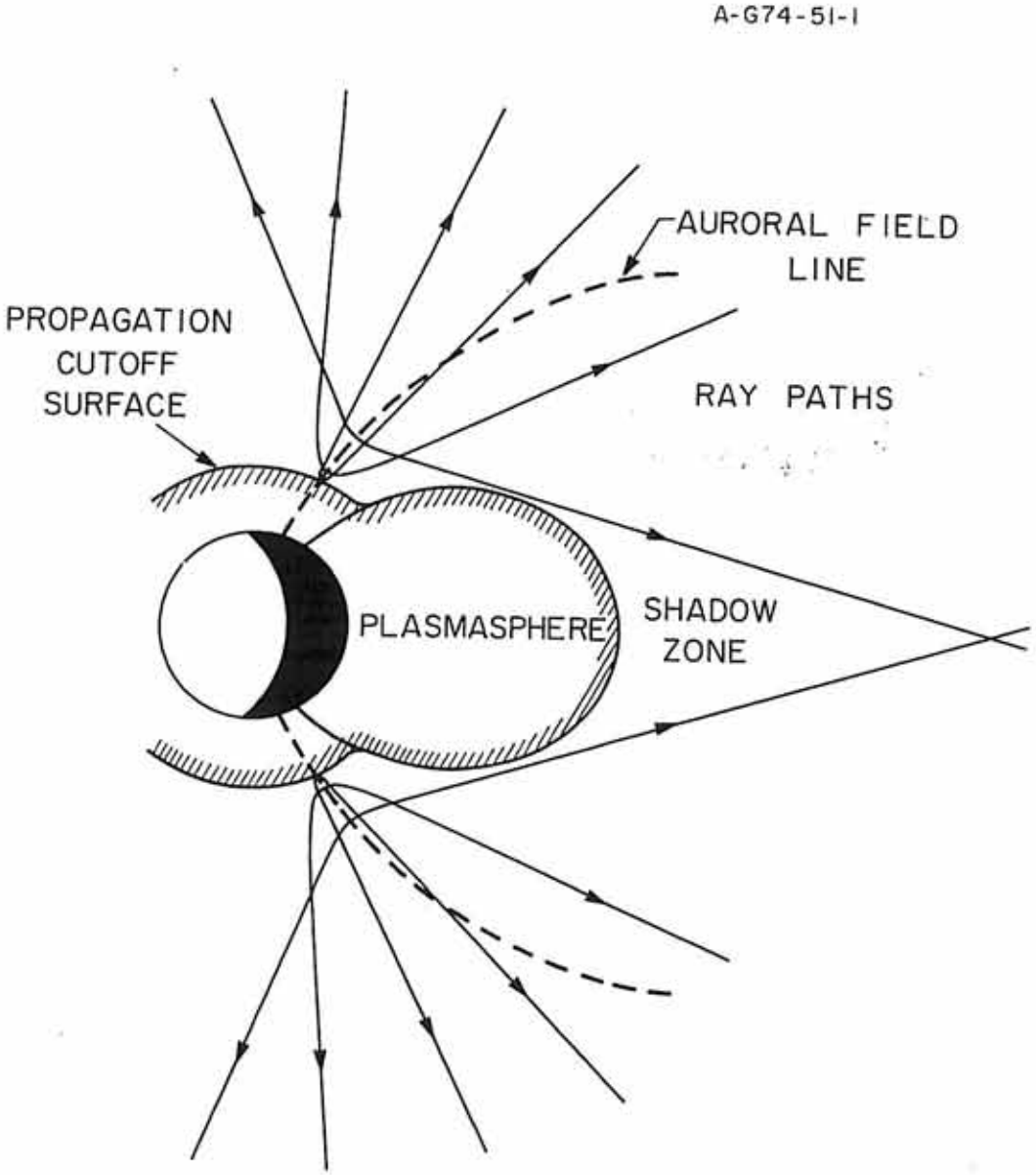
A-G74-51-1
AURORAL FIELD LINE
PROPAGATION CUTOFF SURFACE
RAY PATHS
PLASMASPHERE
SHADOW ZONE

Figure 2

Figure 3 Direction-finding measurements in the northern hemisphere of auroral kilometric radiation at 178 kHz by Kurth et al. [1975]. These directions (lines) are found from the spin modulation in the data obtained by the IMP-8 spacecraft.

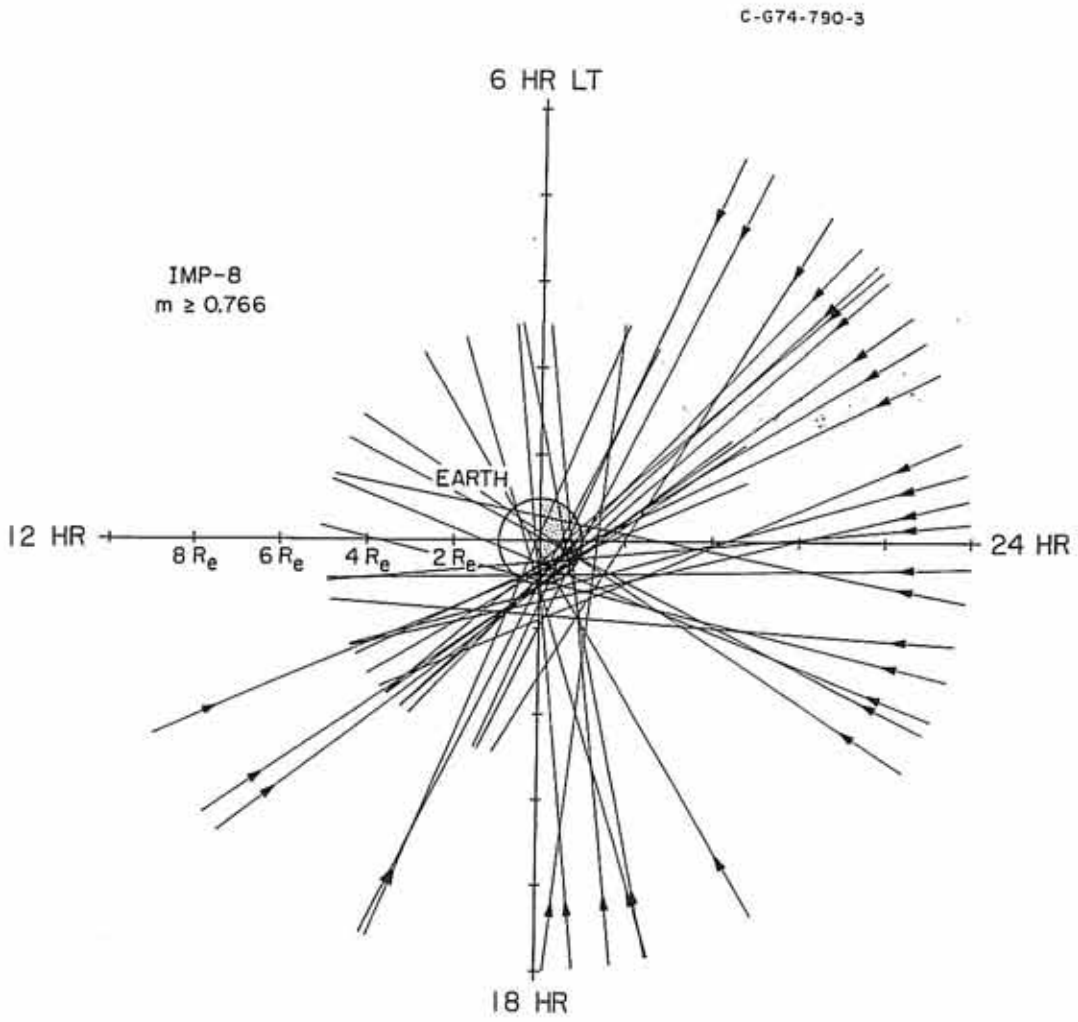
C-G74-790-3
6 HR LT
IMP-8
m ≥ 0.766
EARTH
12 HR
24 HR
8 Re
6 Re
4 Re
2 Re
18 HR

Figure 3

Figure 4 Source centers viewed from over the dawn and dusk terminators projected onto the noon-midnight meridian plane (with +Z the sunlit geomagnetic pole). The overlay is selected field lines from the Mead and Fairfield [1975] magnetic field model MF73D [Alexander and Kaiser, 1976].

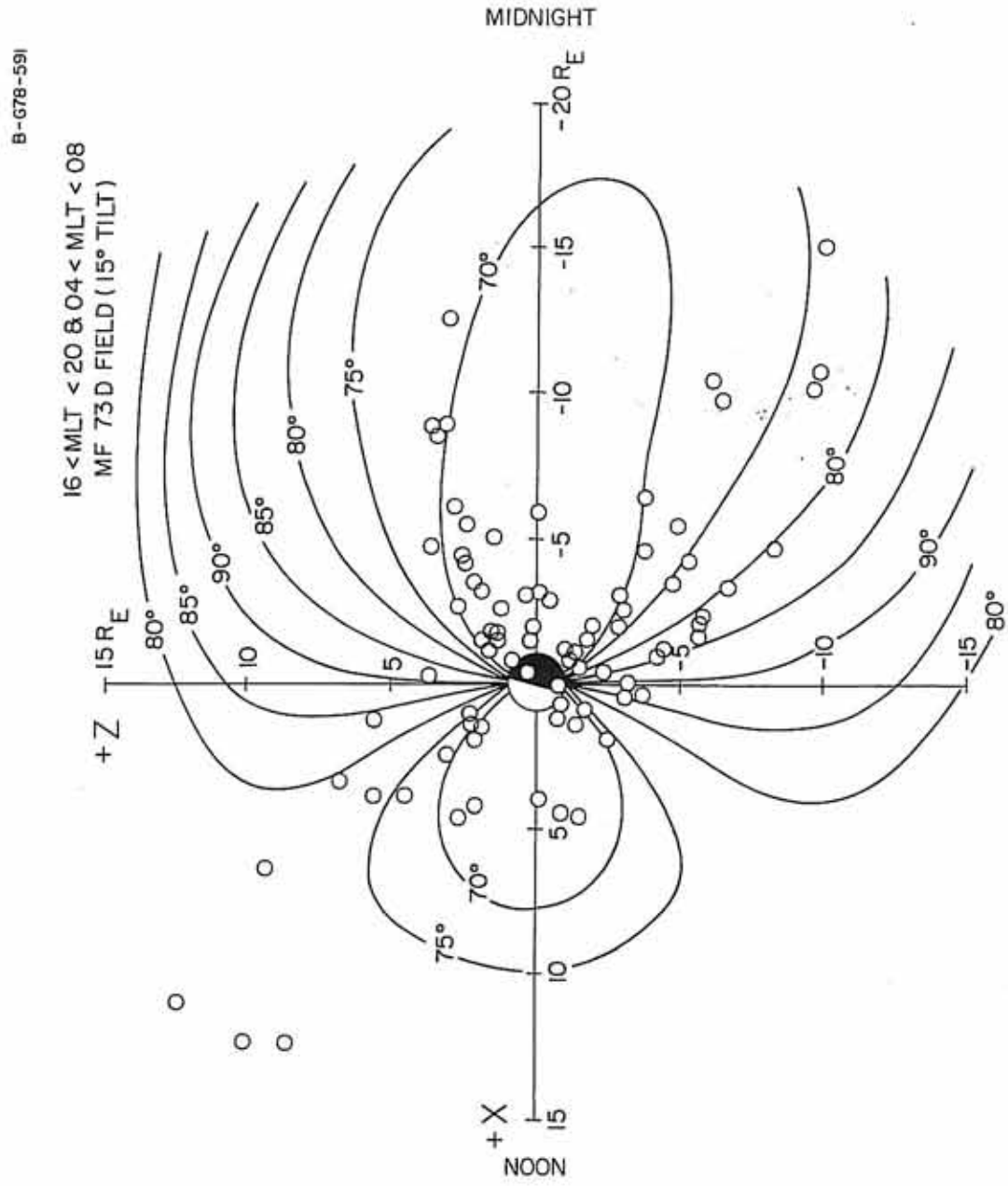
B-G78-591
16 < MLT < 20 & 04 < MLT < 08
MF 73D FIELD (15° TILT)
MIDNIGHT
NOON
+Z
+X
15 R_E
-20 R_E
80°
85°
90°
75°
70°

Figure 4

Figure 5 Combined orbital coverage of Hawkeye-1 and IMP-6. All points on the nightside have been rotated in MLT to form the right side of the figure and all points on the dayside have been rotated in MLT to form the left side of the figure.

B-G78-213

COMBINED ORBITAL COVERAGE OF HAWKEYE-I AND IMP-6

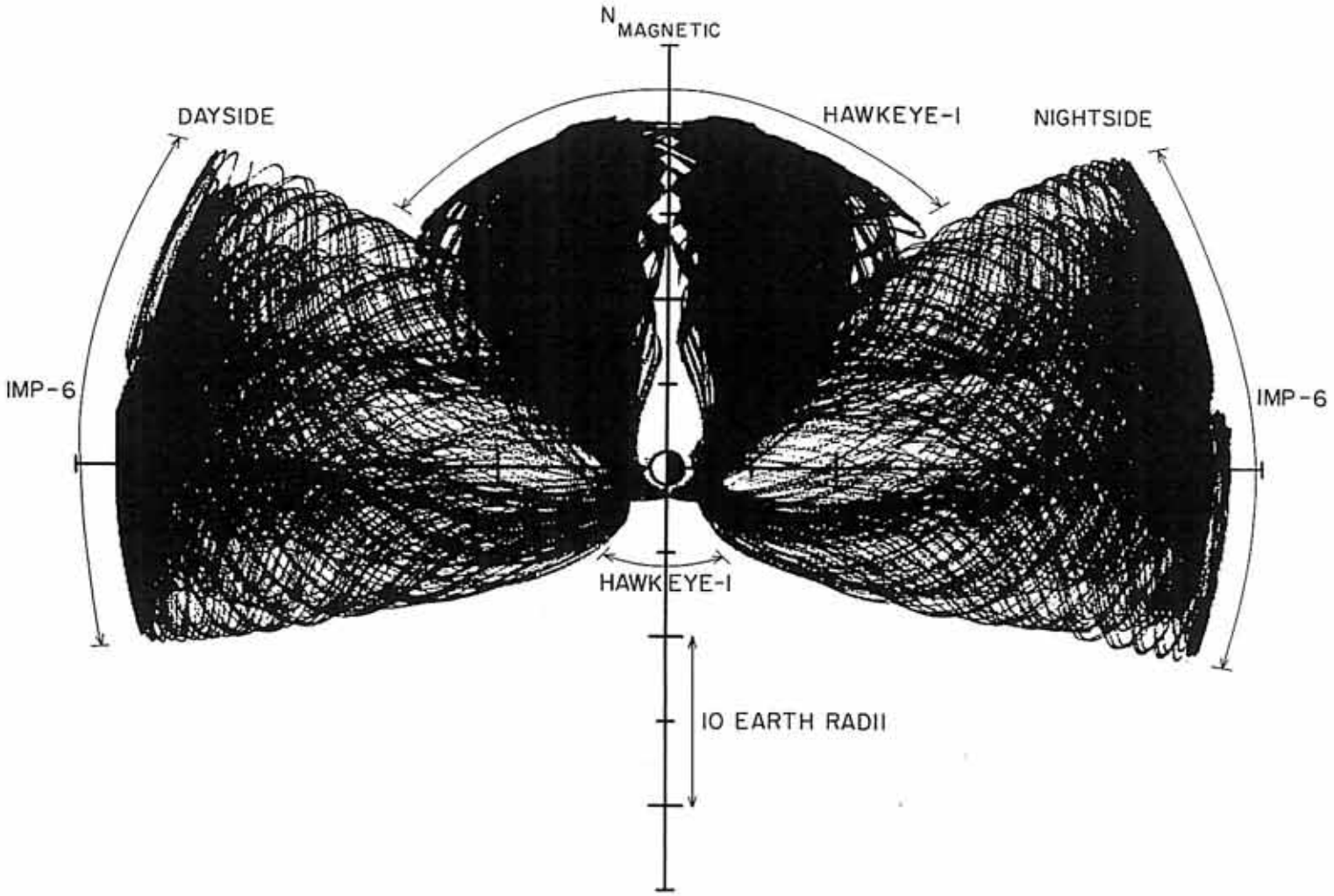

Figure 5

Figure 6 The integration of poynting flux over concentric, earth-centered, spherical shells for model AKR sources is shown. Poynting flux magnitudes must be approximated by measurements of spectral power flux. P_o corresponds to the total power generated by the sources and R_o approximately marks the radial distance of the sources from the center of the earth.

B-G78-270

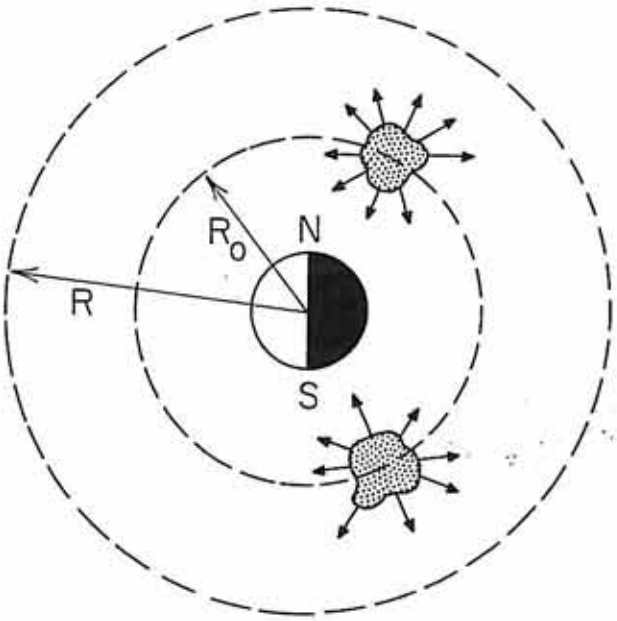

$$P \equiv \int_{\text{SPHERE}} S \cdot dA \approx \sqrt{\frac{\varepsilon_o}{\mu_o}} \frac{1}{\Delta r} \int_{\text{SPHERE}} E^2 dA$$

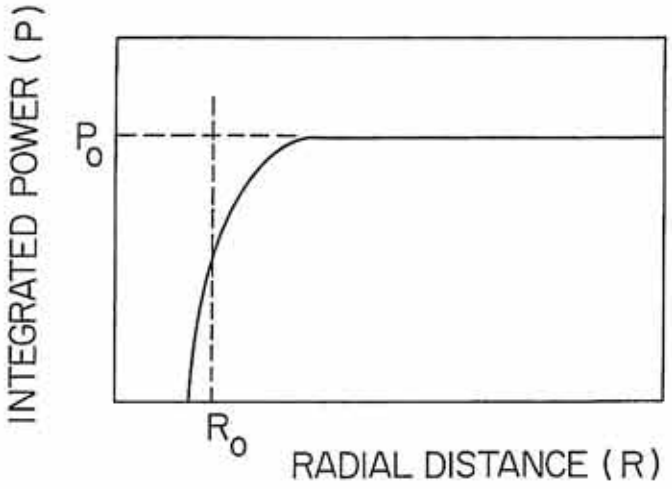

Figure 6

Figure 7 The integration of observed spectral power flux across concentric, earth-centered, spherical shells is shown in the upper graph. The radial distances plotted horizontally correspond to radii of the spherical shells of integration. The lower graph gives the extent of orbital coverage for each spherical surface of integration.

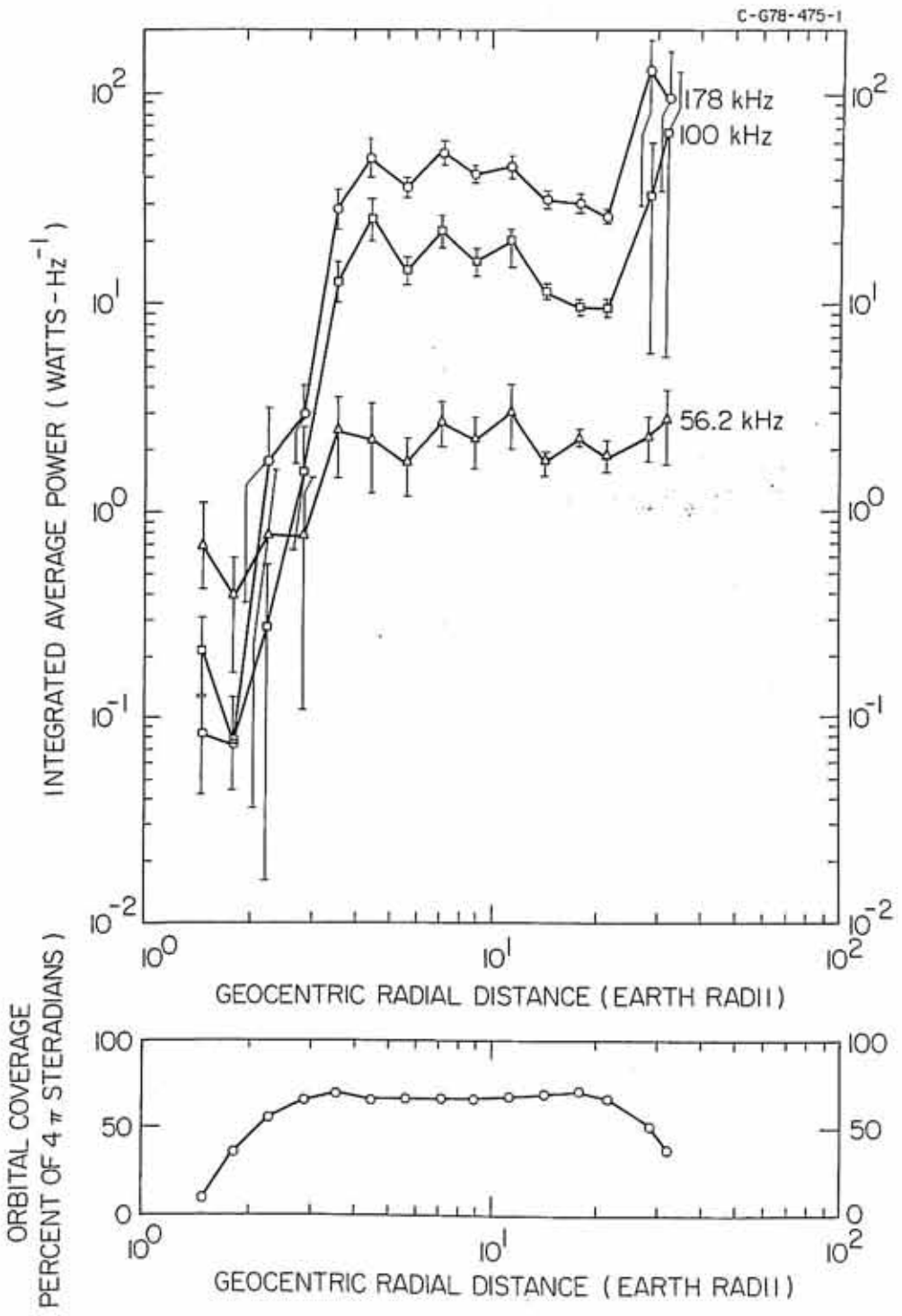
C-G78-475-1
178 kHz
100 kHz
56.2 kHz
INTEGRATED AVERAGE POWER (WATTS - Hz^{-1})
GEOCENTRIC RADIAL DISTANCE (EARTH RADII)
ORBITAL COVERAGE
(PERCENT OF 4 π STERADIANS)
GEOCENTRIC RADIAL DISTANCE (EARTH RADII)

Figure 7

Figure 8 These are intensity modulated polar plots of the average spectral power flux observed in four consecutive, concentric, hemispherical shells at 178 kHz. Dark boarders interior and exterior to each plot mark the limits of orbital coverage. Plotted intensities are derived from the logarithm of spectral power flux.

D-G78-221

POLAR PLOTS OF AVERAGE POWER AT 178 K Hz

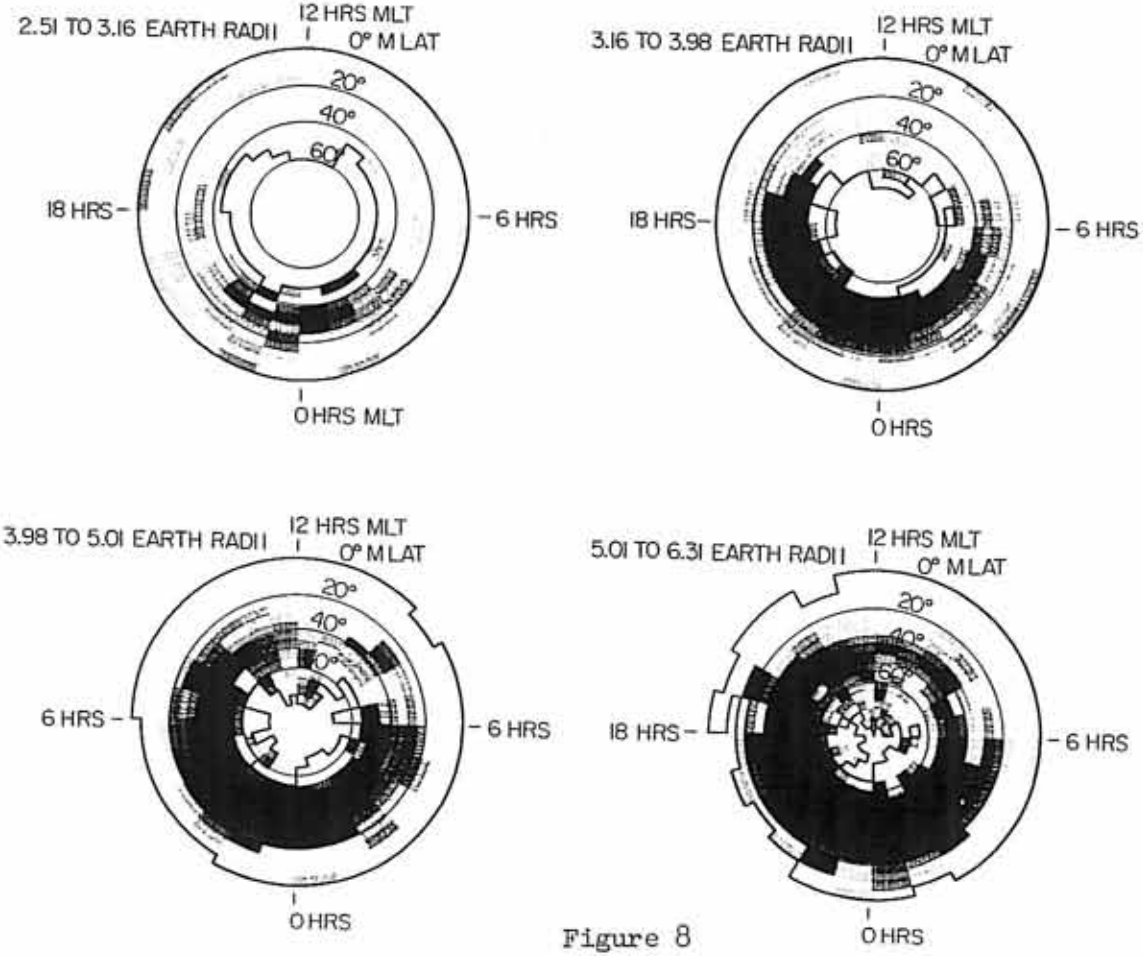

Figure 8

Figure 9 Spectral power at 178 kHz which has been integrated from 30° to 55° λ_m is plotted logarithmically against magnetic local time. The baseline for each plot corresponds to 1.7×10^{-20} Watts/Hz. The shaded regions roughly describe those magnetic local times into which auroral kilometric radiation is beamed.

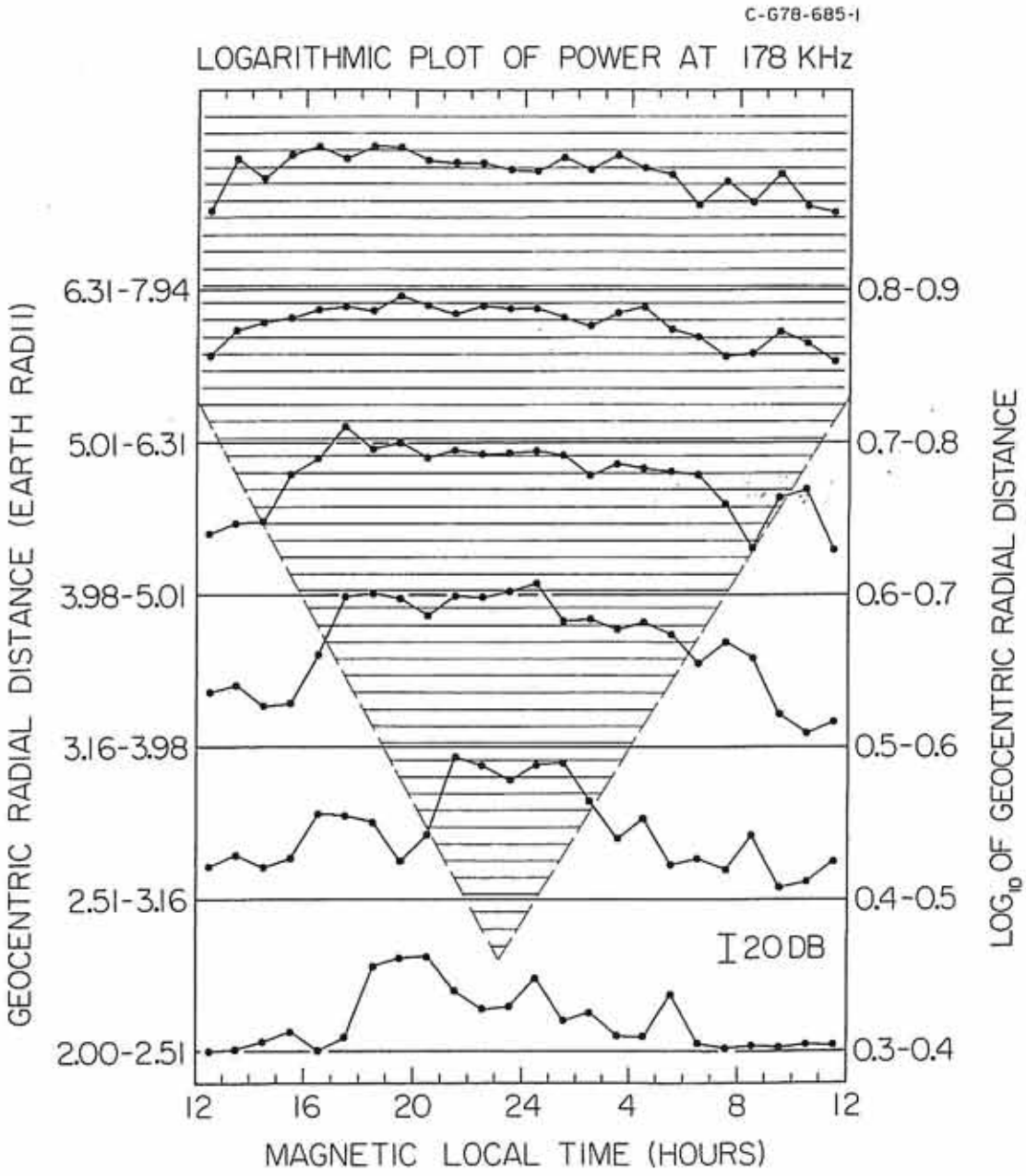
C-G78-685-1
LOGARITHMIC PLOT OF POWER AT 178 KHz
GEOCENTRIC RADIAL DISTANCE (EARTH RADII)
6.31-7.94
5.01-6.31
3.98-5.01
3.16-3.98
2.51-3.16
2.00-2.51
0.8-0.9
0.7-0.8
0.6-0.7
0.5-0.6
0.4-0.5
0.3-0.4
LOG10 OF GEOCENTRIC RADIAL DISTANCE
20 DB
12
16
20
24
4
8
12
MAGNETIC LOCAL TIME (HOURS)

Figure 9

Figure 10 Spectral power at 100 kHz which has been integrated from 30° to 55° λ_m is plotted logarithmically against magnetic local time. The baseline for each plot corresponds to 1.9×10^{-20} Watts/Hz. The shaded regions roughly describe those magnetic local times into which auroral kilometric radiation is beamed.

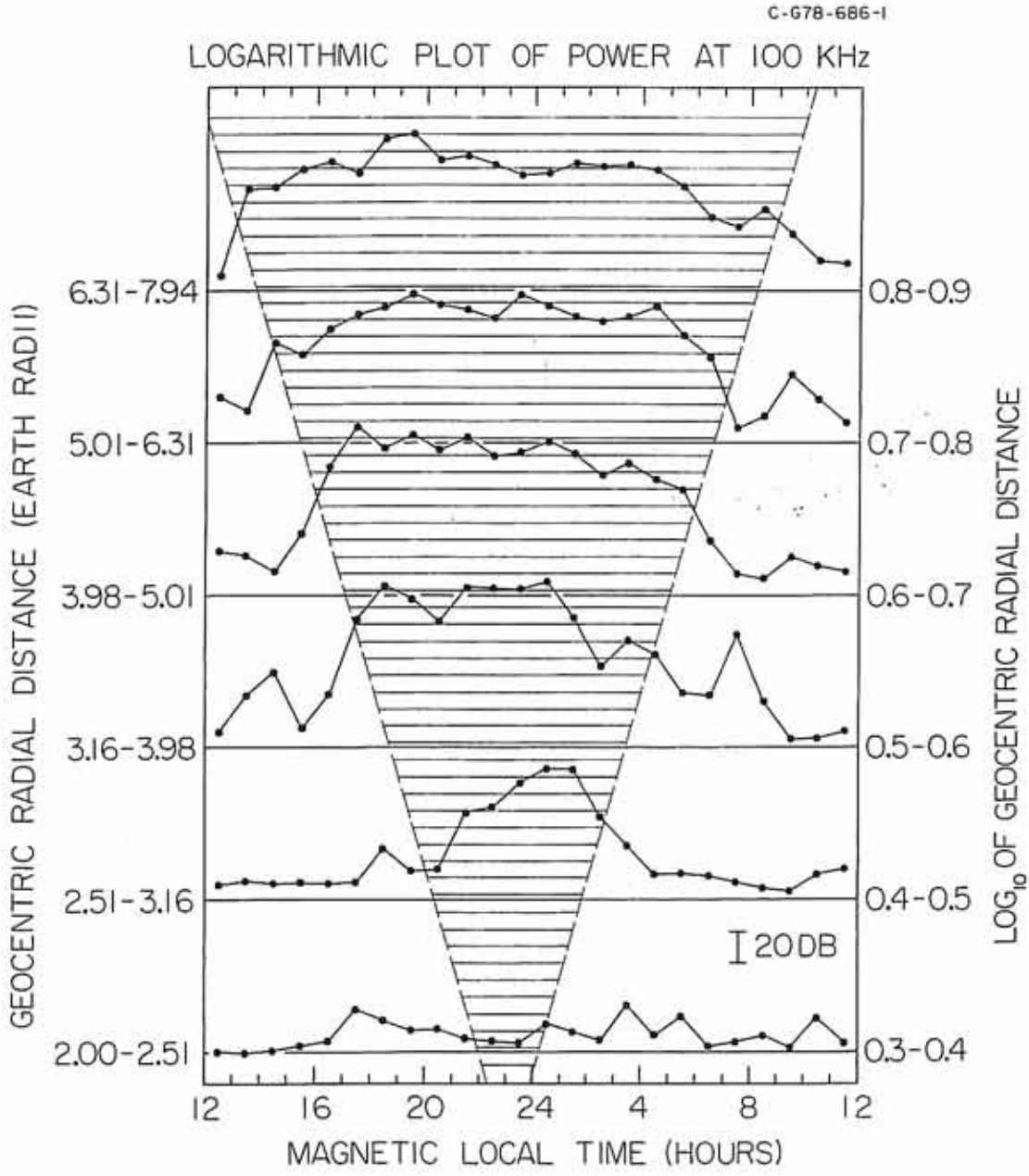
C-G78-686-I
LOGARITHMIC PLOT OF POWER AT 100 KHz
GEOCENTRIC RADIAL DISTANCE (EARTH RADII)
6.31-7.94
5.01-6.31
3.98-5.01
3.16-3.98
2.51-3.16
2.00-2.51
0.8-0.9
0.7-0.8
0.6-0.7
0.5-0.6
0.4-0.5
0.3-0.4
LOG10 OF GEOCENTRIC RADIAL DISTANCE
20DB
12
16
20
24
4
8
12
MAGNETIC LOCAL TIME (HOURS)

Figure 10

Figure 11 Spectral power at 56.2 kHz which has been integrated from 30° to 55° λ_m is plotted logarithmically against magnetic local time. The baseline for each plot corresponds to 2.2×10^{-20} Watts/Hz. The shaded regions roughly describe those magnetic local times into which auroral kilometric radiation is beamed.

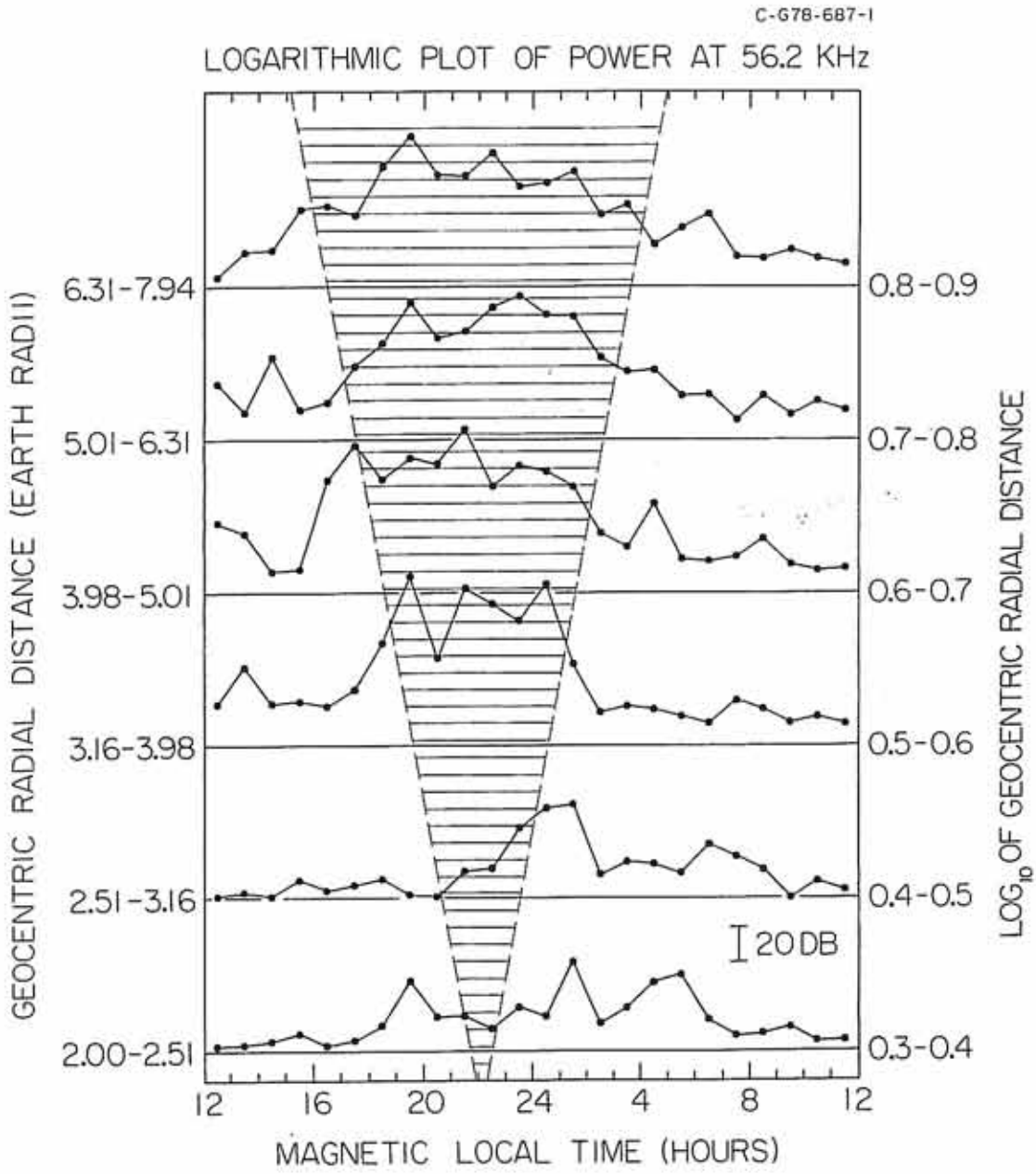
C-G78-687-1
LOGARITHMIC PLOT OF POWER AT 56.2 KHz
GEOCENTRIC RADIAL DISTANCE (EARTH RADII)
6.31-7.94
5.01-6.31
3.98-5.01
3.16-3.98
2.51-3.16
2.00-2.51
0.8-0.9
0.7-0.8
0.6-0.7
0.5-0.6
0.4-0.5
0.3-0.4
LOG10 OF GEOCENTRIC RADIAL DISTANCE
20 DB
12
16
20
24
4
8
12
MAGNETIC LOCAL TIME (HOURS)

Figure 11

Figure 12 Average spectral power flux is plotted against geocentric radial distance in four magnetic local time groups. Spectral power has been averaged between 30° and 55° λ_m in each magnetic local time group. The graph from 22^h to 24^h MLT best corresponds to the MLT of the source region of auroral kilometric radiation.

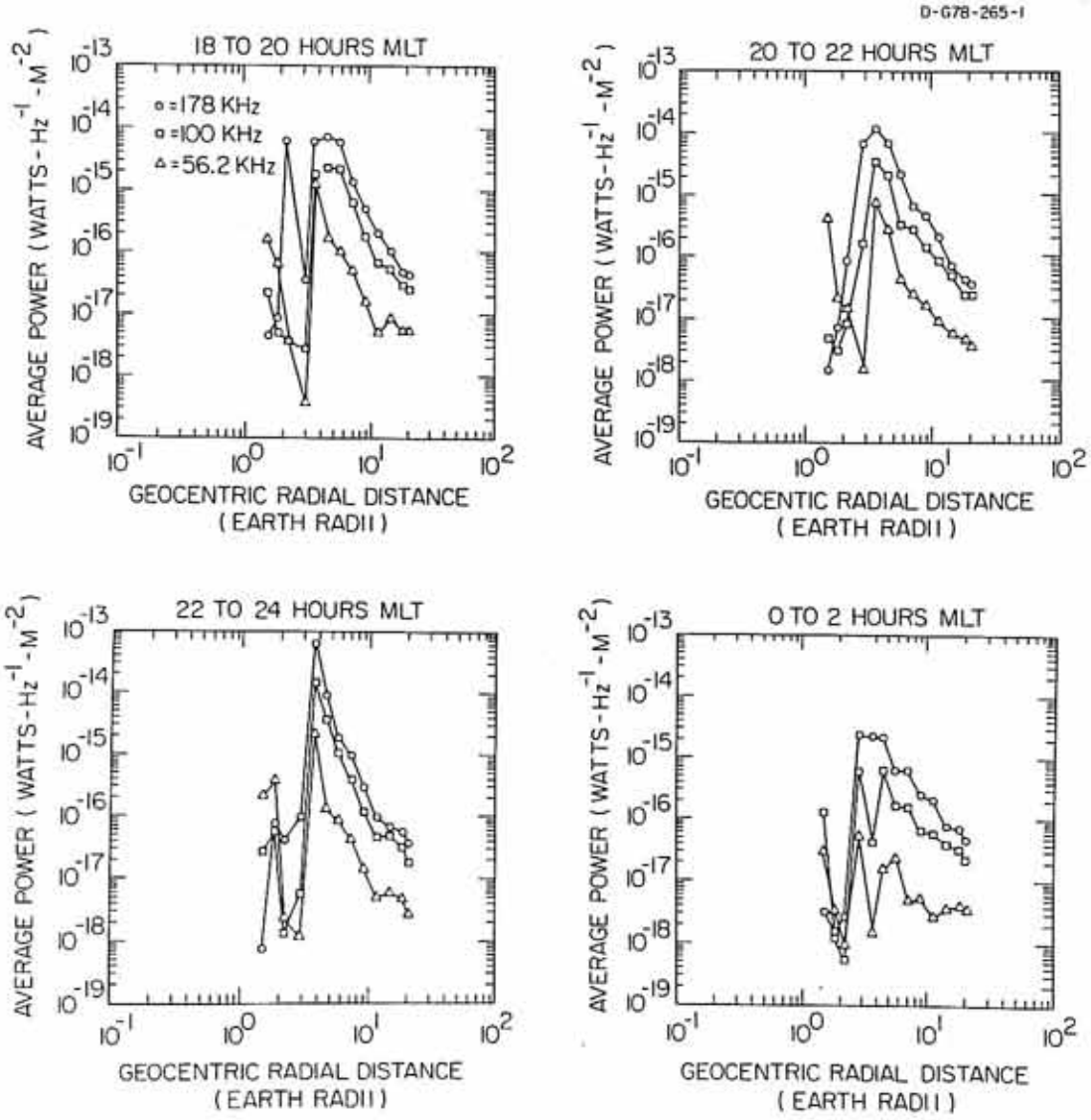
D-G78-265-I
18 TO 20 HOURS MLT
o = 178 KHz
o = 100 KHz
Δ = 56.2 KHz
AVERAGE POWER (WATTS - Hz^{-1} - M^{-2})
GEOCENTRIC RADIAL DISTANCE
(EARTH RADII)
20 TO 22 HOURS MLT
GEOCENTIC RADIAL DISTANCE
(EARTH RADII)
22 TO 24 HOURS MLT
GEOCENTRIC RADIAL DISTANCE
(EARTH RADII)
0 TO 2 HOURS MLT
GEOCENTRIC RADIAL DISTANCE
(EARTH RADII)

Figure 12

Figure 13 Average spectral power flux is plotted against the distances from selected possible source locations. All four plots are for spectral power flux which has been averaged between 22^h and 24^h MLT and between 30° and 55° λ_m. Data in the upper left panel is plotted against geocentric radial distances. Points in the other three panels are plotted as a function of the distances away from model source locations at 2, 3, and 4 R_e. The dotted lines which indicate a $1/R^2$ slope show that data plotted for a source location at 3 R_e most nearly follows the $1/R^2$ functional dependence.

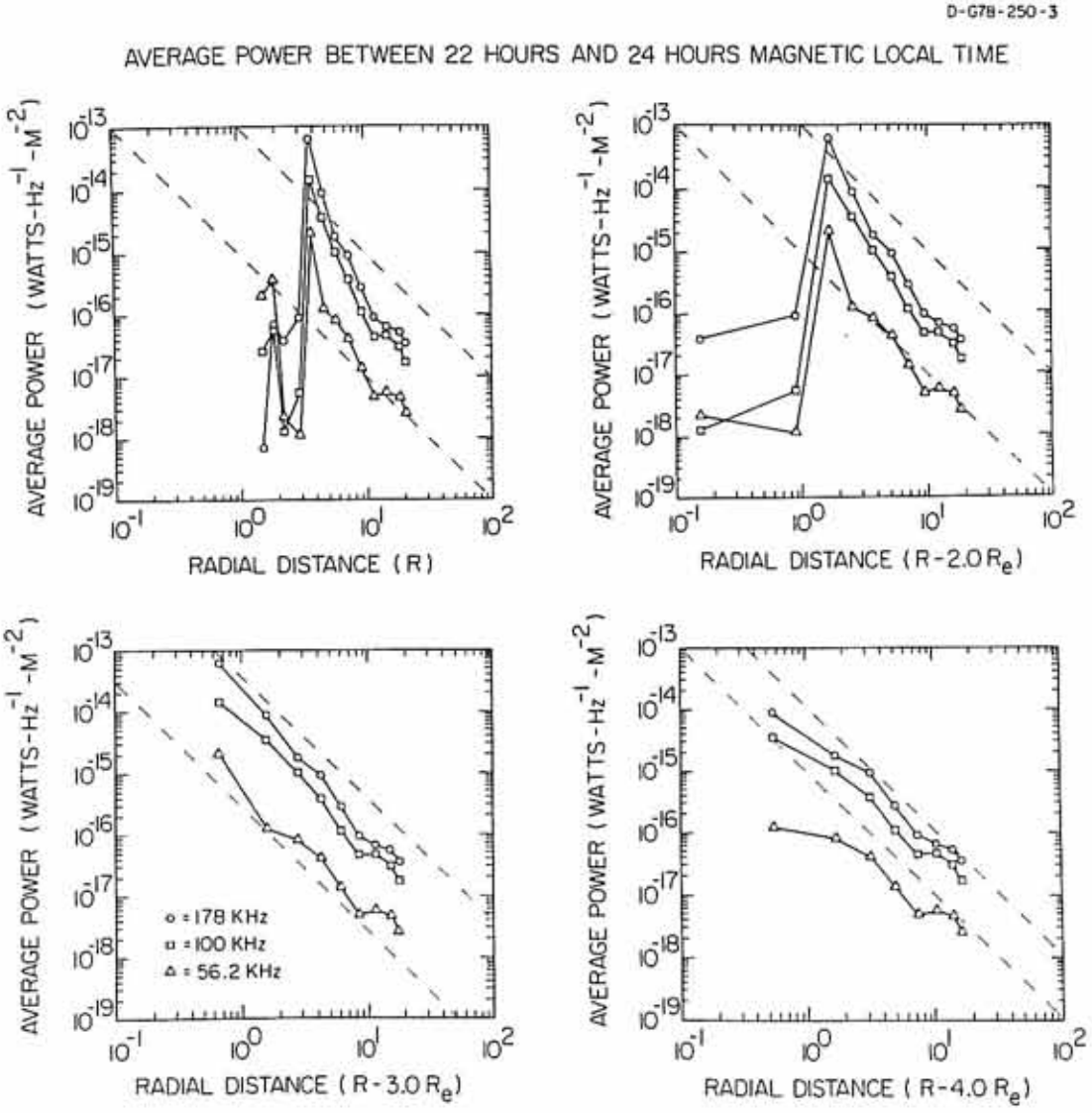
D-G78-250-3
AVERAGE POWER BETWEEN 22 HOURS AND 24 HOURS MAGNETIC LOCAL TIME
AVERAGE POWER (WATTS-Hz^{-1}-M^{-2})
RADIAL DISTANCE (R)
RADIAL DISTANCE (R-2.0 R_e)
RADIAL DISTANCE (R-3.0 R_e)
RADIAL DISTANCE (R-4.0 R_e)
o = 178 KHz
□ = 100 KHz
Δ = 56.2 KHz
R = GEOCENTRIC RADIAL DISTANCE IN EARTH RADII
R_e = EARTH RADIUS

Figure 13

Figure 14 The slopes of straight line fits to the data are plotted against the geocentric distances of model source positions. Spectral power flux falls off as $1/R^2$ for a model source positioned between 2 and 3 R_e.

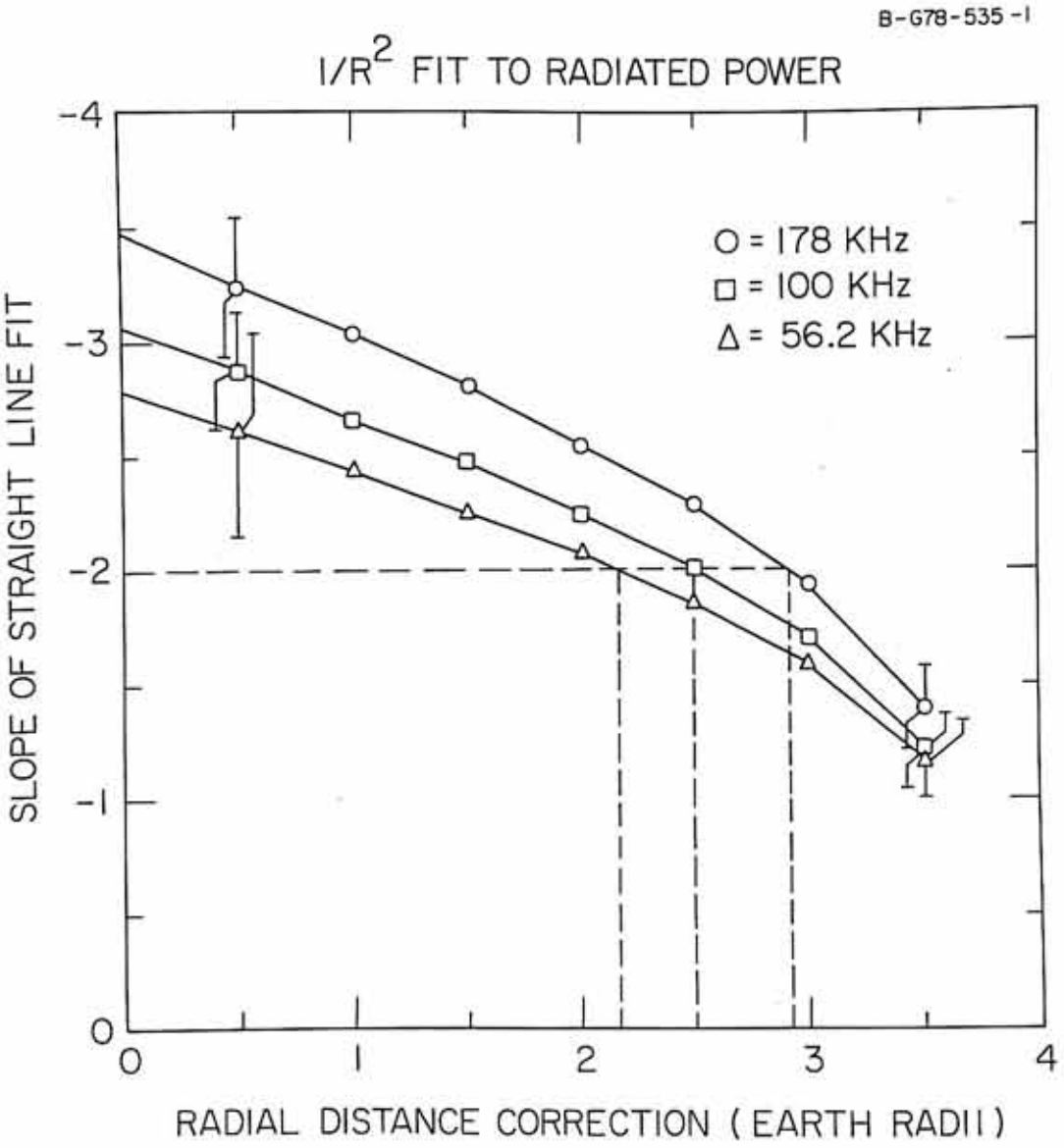
B-G78-535-1
1/R2 FIT TO RADIATED POWER
O = 178 KHz
□ = 100 KHz
Δ = 56.2 KHz
SLOPE OF STRAIGHT LINE FIT
-4
-3
-2
-1
0
0
1
2
3
4
RADIAL DISTANCE CORRECTION (EARTH RADII)

Figure 14

Figure 15 The time average extent of the cone-like emission of AKR is shown against the Hawkeye magnetic field model of Chen [1978]. On the average, both sources are observable in the equatorial plane on the nightside of the earth at a distance of 12 R_e and beyond. The polar cusp is illuminated by AKR at radial distances as close as 4 R_e.

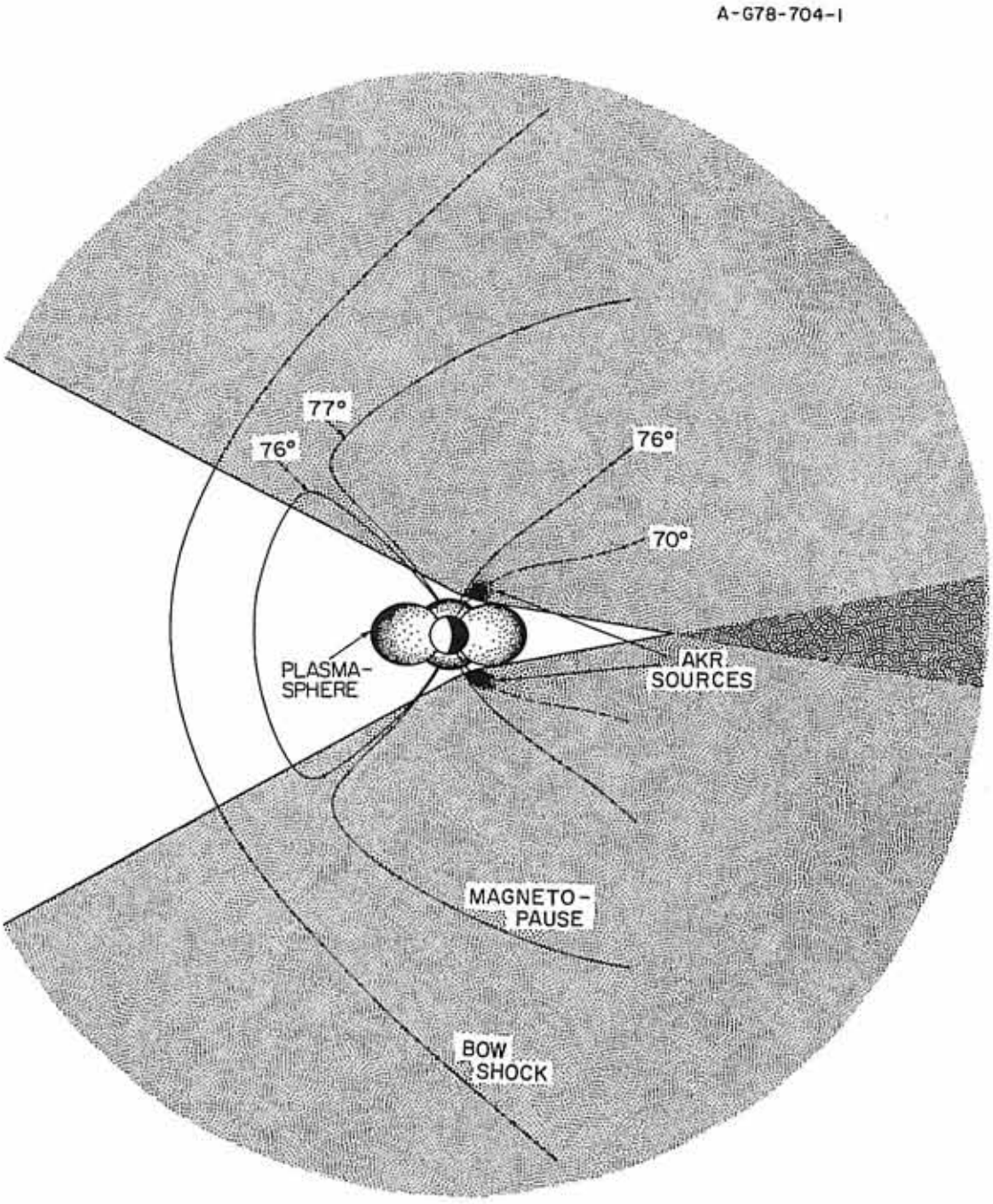
A-G78-704-I
77°
76°
76°
70°
PLASMA-
SPHERE
AKR
SOURCES
MAGNETO-
PAUSE
BOW
SHOCK

Figure 15